Journal of Power Sources 195 (2010) 7359–7369

Contents lists available at ScienceDirect

Journal of Power Sources

journal homepage: www.elsevier.com/locate/jpowsour

High performance proton exchange membrane fuel cell electrode assemblies

Tien-Fu Yang[a], Lih-Wu Hourng[a], T. Leon Yu[b,c,*], Pei-Hung Chi[c], Ay Su[c]

[a] Department of Mechanical Engineering, National Central University, Chung-Li, Taoyuan 32001, Taiwan
[b] Department of Chemical Engineering & Materials Science, Yuan Ze University, Nei-Li, Chung-Li, Taoyuan 32003, Taiwan
[c] Fuel Cell Center, Yuan Ze University, Nei-Li, Chung-Li, Taoyuan 32003, Taiwan

ARTICLE INFO

Article history:
Received 3 April 2010
Accepted 16 April 2010
Available online 31 May 2010

Keywords:
Fuel cell
Membrane electrode assembly
Catalyst layer

ABSTRACT

The conventional 5-layer membrane electrode assembly (MEA) consists of a proton exchange membrane (PEM) locating at its center, two layers of Pt-C-40 (Pt content 40 wt%) locating next on both surfaces of PEM, and two gas diffusion layers (GDL) locating next on the outer surfaces of Pt-C layers (structure-a MEA). In this paper, we report three modified MEAs consisting of Pt-C-40 (Pt content 40 wt%) and Pt-C-80 (Pt content 80 wt%) catalysts. These are: (1) 7-layer structure-b MEA with a thin Pt-C-80 layer locating between Pt-C-40 layer and PEM; (2) 7-layer structure-c MEA with a thin Pt-C-80 layer locating between Pt-C-40 layer and GDL; and (3) 5-layer structure-d MEA with Pt-C-40 and Pt-C-80 mixing homogeneously and locating between PEM and GDL. Under a fixed Pt loading, we find structure-b, -c, and -d MEAs with 20–40 wt% Pt contributed from Pt-C-80 have better fuel cell performance than structure-a MEA consisting only of Pt-C-40. The reasons for the better fuel cell performance of these modified MEAs are attributed to the better feasibility for O_2 gas to reach cathode Pt particles and lower proton transport resistance in catalyst layers of the modified MEAs than structure-a MEA.

1. Introduction

It is generally accepted that proton exchange membrane (PEM) fuel cells present an attractive alternative to traditional power sources, due to their high efficiency and non-pollution. However, the high cost of the cell components causes impediment to their commercialization. One of the primary contributors to the PEM fuel cell (PEMFC) high cost is the catalyst, i.e. platinum (Pt). In the past two decades, lots of researchers made efforts to find cheaper metals to replace the expensive Pt as fuel cells catalysts [1,2]. However till now, Pt is still widely used as catalyst in fuel cells due to its high catalytic activity and high stability.

One of the methods to reduce the catalyst cost of PEMFC is to improve the utilization of Pt catalysts. The most common method for fabricating the PEMFC catalyst layer is to mix the Pt-C (carbon powder supported Pt) agglomerates with solubilised polymer electrolytes (for example Nafion ionomer) and apply this paste to a porous carbon support gas diffusion layer (GDL). However, up to 50% of Pt atoms in such electrodes may be inactive [3]. Three important factors controlling catalysts utilization are: (1) catalysis activity of catalysts particles; (2) proton transport resistance in the catalyst layers; (3) the contact frequency of fuel and oxidant gases (O_2 or air) with catalysts particles, especially when operating at high currents.

Factor-1 depends on the specific surface area of catalysts particles, the Pt particles with higher specific surface area should have higher catalysis activity. Thus factor-1 is mostly controlled by the catalyst particles sizes. Factor-2 depends on the path length for protons transport in the catalyst layer and the ratio of Pt particles in contact with ionic groups of polyelectrolyte binder (for example sulfonic acid groups of Nafion resin). The aggregate ionic groups of polyelectrolyte binder form pathways facilitating proton transport in catalyst layer. It is necessary that Pt atoms are in contact with ionic groups of polyelectrolyte binders. The proton produced on the surfaces of Pt particles can be transported via the ionic groups aggregation pathways [4,5]. The proton transport path length depends on the thickness of catalyst layer. Increasing catalyst layer thickness results in an increase in proton transport path length in catalyst layer and thus an increase in proton transport resistance. Thus factor-2 is controlled by the optimum wt ratio of [Pt]/[polyelectrolyte binder] and the thickness of catalyst layer. Factor-3 depends on the concentrations of H_2 and O_2 molecules in the catalyst layers, and the diffusivity of H_2 and O_2 molecules in the catalyst layers, and is thus controlled by the H_2 and O_2 flow rates, the structure of catalyst layer, and the porosity of catalyst layer. Usually the diffusivity of O_2 molecules in cathode is much lower than that of H_2 molecules in anode, the "feasibility of O_2 molecules to reach catalyst particles in cathode" is more important than that of H_2 molecules in anode.

* Corresponding author at: Department of Chemical Engineering & Materials Science, Yuan Ze University, 135 Yuan-Tong Rd., Nei-Li, Chung-Li, Taoyuan 32003, Taiwan. Tel.: +886 3 4638800x2553; fax: +886 3 4559373.
E-mail address: cetlyu@saturn.yzu.edu.tw (T.L. Yu).

0378-7753/$ – see front matter © 2010 Published by Elsevier B.V.
doi:10.1016/j.jpowsour.2010.04.063

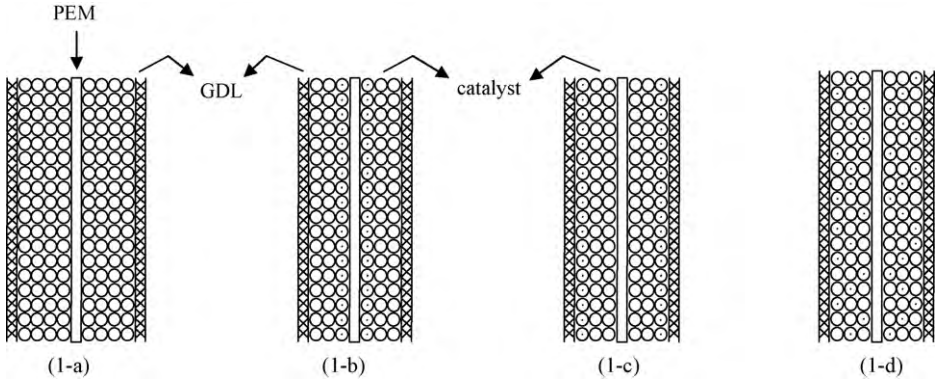

Fig. 1. Structures of membrane electrode assemblies (MEA). (a) 5-layer conventional MEA with Pt-C-40 (40 wt% Pt) catalysts layer locating between PEM and GDL; (b) 7-layer MEA with a Pt-C-80 (80 wt% Pt) layer locating near PEM and a Pt-C-40 layer locating near GDL; (c) 7-layer MEA with a Pt-C-80 layer locating near GDL and a Pt-C-40 layer locating near PEM; (d) 5-layer MEA with Pt-C-80 and Pt-C-40 mixed homogeneously and locating between PEM and GDL. The Pt loading of each MEA is same, but the thicknesses of Pt-C layers in (b), (c), and (d) are thinner than that in (a). Catalysts: (◯) Pt-C-40; (⊙) Pt-C-80.

In order to improve the utilization of Pt catalysts in a PEMFC, one should (1) increase the catalyst particles surface area, (2) reduce the catalyst layer thickness under an optimum [Pt]/[polyelectrolyte binder] wt ratio, (3) supply sufficient H_2 and O_2 reactants for electrochemical reactions in catalyst layer, and (4) improve the catalyst layer structure to raise the contact frequency of Pt catalyst particles with reactant gas molecules. Thus the structure of the catalyst layer design is important for a MEA to have a high catalyst utilization efficiency.

In the past two decades, several catalyst layer structure designs for PEMFC and DMFC (direct methanol fuel cell) and fabrication methods had been reported in literature [2,4–15]. The most widely used conventional catalyst layer structure is shown in Fig. 1a, which consists of a Pt-C catalyst layer locating between PEM and GDL. The advantage of using Pt-C catalysts is the reduction of nano-Pt particles agglomeration in the catalyst layer, thus avoid reducing Pt catalytic surface area. The carbon powders particles sizes of commercial Pt-C are around 50–80 nm [16] and the particles sizes of Pt deposited on carbon powder surfaces increase from 1.5 nm to 4.9 nm (with Pt specific surface area decreases from 185 $m^2\,g^{-1}$ to 57 $m^2\,g^{-1}$) as the amount of Pt deposited on carbon powders surfaces increases from 5 wt% to 80 wt% [17,18]. The Pt particles sizes increase with increasing Pt deposited quantity on carbon powder surfaces, thus the Pt specific catalytic surface area decreases with increasing the amount of Pt deposited on the carbon powder surfaces [18]. At a fixed Pt loading in a catalyst layer, the fabrication of high Pt content Pt-C powders in a MEA decreases both the Pt catalysis activity and the thickness of the catalyst layer (because of low content of large size carbon particles). Thus both the Pt catalysis activity and the proton transport resistance in catalyst layer decrease with increasing Pt content of Pt-C powders. However, the use of low Pt content Pt-C catalysts in MEA causes increments both in Pt catalytic surface area and thickness of catalyst layer (because of high content of large sizes carbon particles). Thus both the Pt catalytic activity and the proton transport resistance in catalyst layers increase with decreasing Pt content of Pt-C powders. The subject how to obtain "*a MEA with high Pt catalysis activity and low proton transport resistance catalyst layer*" is one of the important issues for MEA catalyst layer structure design and fabrication. Most of researchers use Pt-C particles containing 40–50 wt% of Pt (Pt particles sizes around 2.9–3.3 nm and specific surface area around 110–86 $m^2\,g^{-1}$) as catalysts in PEMFC. At a fixed Pt loading, a MEA consisting of Pt-C catalysts with 40–50 wt% of Pt content has a medium Pt catalytic surface area and a medium catalyst layer thickness, and thus an optimum PEMFC performance can be obtained.

An improvement of fuel cell power output by modifying catalyst layer structure had been reported [9,19,20]. Its structure is similar to Fig. 1a, instead of using Pt-C-40 (Pt content 40 wt%, Pt particles sizes ~2.8 nm and specific surface area ~100 $m^2\,g^{-1}$) the authors used Pt-C-20 (Pt content 20 wt%, Pt particles sizes ~2.2 nm and specific surface area ~128 $m^2\,g^{-1}$) as major catalysts and with an additional sputtered Pt thin film locating between PEM and Pt-C-20 layer [9,19,20]. These authors reported that sputtering one additional Pt thin film with a Pt loading of 0.05 mg cm^{-2} at the interface between Pt-C-20 layer and PEM (the total Pt loading was 0.45 mg cm^{-2}) could enhance fuel cell output power of Fig. 1a MEA which consisted of only one Pt-C-20 catalyst layer with a Pt loading of 0.40 mg cm^{-2}. One of the reasons of higher output power of this modified MEA than Fig. 1a MEA could be due to the higher total Pt loading of the modified MEA. The main disadvantage of the catalyst layer design of the modified MEA is the increase of catalyst cost by sputtering an additional Pt thin film in Fig. 1a MEA.

In this paper, we modify Fig. 1a MEA and propose three MEA structures: (1) in addition to Pt-C-40 catalyst layer, coating a high Pt content Pt-C-80 (Pt content 80 wt%, Pt particle sizes ~4.9 nm and specific surface area ~57 $m^2\,g^{-1}$) thin catalyst layer at the interface between Pt-C-40 layer and PEM (Fig. 1b); (2) in addition to Pt-C-40 catalyst layer, coating a thin Pt-C-80 layer at the interface between Pt-C-40 layer and GDL (Fig. 1c); (3) coating a catalyst layer consisting of homogeneous mixture of Pt-C-40 and Pt-C-80 between PEM and GDL (Fig. 1d). The quantities of Pt-C-40 in Fig. 1b–d MEAs were lower than that of Fig. 1a MEA and the reduced amount of Pt loading of Pt-C-40 was equal to the increased amount of Pt loading of Pt-C-80. Thus the total amount of Pt loadings of unmodified Fig. 1a MEA and of modified Fig. 1b–d MEAs were fixed at a same Pt loading quantity. The main purpose of this study is to replace 10–40 wt% of Pt-C-40 with thin layers of Pt-C-80 and thus reduce the content of large sizes carbon support powders and the thickness of catalyst layers. The lower thickness of catalyst layer results in a lower proton transport resistance in catalyst layers and a higher efficiency for O_2 molecules to reach the cathode Pt catalytic sites, particularly when the fuel cell is operated at a high current. The replacement of 10–40 wt% of Pt-C-40 with Pt-C-80 causes a little loss of Pt particles surface area. The loss of Pt catalysis activity can be overcome by the reduction of proton transport resistance and the improvement of the feasibility of the reactants gases to reach the electro-catalytic sites. The advantage of using large Pt-C-80 particles (carbon particle sizes 50–80 nm) instead of using nano-Pt particles as mentioned in Refs. [9,19,20] is the avoiding of inserting nano-Pt particles (particle sizes 5.0–5.5 nm; specific surface area 20–25 $m^2\,g^{-1}$) into the voids of GDL (i.e. carbon paper) when fabricating Pt particle thin layer near GDL. The insertion of Pt nano-particles into voids of GDL causes the blockage of fuel (H_2) and oxidant (O_2) gases flows, leading to a poor fuel cell performance. Another advantage of using

Table 1
The catalysts loadings of structure-a, -b, -c, and -d MEAs. Total Pt loadings of MEA-1–MEA-10 are 0.5 mg cm^{-2} at anode and 1.0 mg cm^{-2} at cathode. Total Pt Loadings of MEA-11–MEA-13 are 0.3 mg cm^{-2} at anode and 0.6 mg cm^{-2} at cathode.

MEA structure	MEA no	Anode (mg cm^{-2})			Cathode (mg cm^{-2})		
		Pt-C-80 near GDL	Pt-C-40	Pt-C-80 near PEM	Pt-C-80 near PEM	Pt-C-40	Pt-C-80 near GDL
a	1	–	1.250	–	–	2.500	–
b	2	–	1.125	0.0625	0.125	2.250	–
b	3	–	1.000	0.125	0.250	2.000	–
b	4	–	0.750	0.250	0.500	1.500	–
c	5	0.0625	1.125	–	–	2.250	0.125
c	6	0.125	1.000	–	–	2.000	0.250
c	7	0.250	0.750	–	–	1.500	0.500
d	8		Pt-C-80 = 0.0625 Pt-C-40 = 1.125			Pt-C-80 = 0.125 Pt-C-40 = 2.250	
d	9		Pt-C-80 = 0.125 Pt-C-40 = 1.000			Pt-C-80 = 0.250 Pt-C-40 = 2.000	
d	10		Pt-C-80 = 0.250 Pt-C-40 = 0.750			Pt-C-80 = 0.500 Pt-C-40 = 1.500	
a	11	–	0.750	–	–	1.500	–
c	12	0.0625	0.625	–	–	1.250	0.125
ac	13	–	0.750	–	–	1.250	0.125

Pt-C-80 instead of using Pt nano-particles is the higher Pt active surface area of Pt-C-80 than Pt nano-particles.

2. Experimental

2.1. Materials

The Nafion solution (DuPont Co) was a 5 wt% Nafion (EW = 1100) diluted in a mixture solvent containing water, 2-propanol, methanol, and unspecified ethers [21]. The PEM was Nafion-212 (thickness ~50 μm, DuPont Co). The gas diffusion layer (GDL) was a carbon paper (SGL-35BC, SGL Co, Germany). The Pt-C-40 (Pt content 40 wt%, particle sizes 2.8 nm and specific surface area 100 m^2 g^{-1}) and Pt-C-80 (Pt content 80 wt%, particle sizes 4.9 nm and specific surface area 57 m^2 g^{-1}) catalysts were purchased from E-Tek Co.

2.2. Preparation of PEMFC membrane electrode assembly (MEA)

Before MEA preparation, the Nafion-212 membrane was treated at 70 °C in 5 wt% H_2O_2 aqueous solution for 1 h, followed in distilled water for 1 h, in 1 M H_2SO_4 solution for 1 h, and subsequently in distilled water for 15 min. The Pt-C catalyst pastes were prepared by mixing Pt-C powder in an isopropanol/water (1/9 g/g) solution and stirred mechanically for 30 min to give a homogeneous mixture. Subsequently, Nafion solution was added into the mixture and stirred by ultrasound for 1 h. The MEAs were prepared by spraying the Pt-C-80 and Pt-C-40 catalyst pastes layer by layer upon GDL according to the structure designs shown in Fig. 1 and dried in air at ~80 °C for 2 h, and subsequently dried at ~80 °C under vacuum for 30 min. The final wt ratio of [Pt-C]/[Nafion solid resin] on GDL was ~2/1. The Nafion membrane was sandwiched between anode and cathode electrodes and hot pressed at 135 °C with 50 kg cm^{-2} for 30 s and followed with 100 kg cm^{-2} for 1 min. Thirteen MEAs in which MEA#1–MEA#10 consisting of anode/cathode Pt loadings of 0.5 mg cm^{-2}/1.0 mg cm^{-2} and MEA#11–MEA#13 consisting of anode/cathode Pt loadings of 0.3 mg cm^{-2}/0.6 mg cm^{-2} were prepared in this work. The catalyst layer structure designs and Pt-C-40 and Pt-C-80 loadings of these MEAs are summarized in Table 1. In Table 1, the structure designations a–d are same as the designations shown in Fig. 1. In Table 1, the PEM is assumed to be located in the middle, i.e. between anode and cathode, and the Pt-C catalyst loading of each catalyst layer on both sides of PEM is listed sequentially from PEM in the middle to the outside layers according to the MEA structure. The structure designation d of Table 1 indicates the Pt-C-40 and Pt-C-80 particles were homogeneously mixed and located between PEM and GDL, and the structure designation ac of Table 1 indicates the anode catalyst layer consists of only Pt-C-40, i.e. similar to a-structure, and the cathode catalyst layer consists of Pt-C-40 and Pt-C-80 layers with Pt-C-80 layer locating near GDL, i.e. similar to c-structure.

2.3. PEMFC unit cell performance test

The performances of PEMFC unit cells of MEAs with various catalyst layer structures were tested under ambient pressure using a Model 850C Compact Fuel Cell Test Station (Scribner Associates, Inc.). The anode, cell, and cathode temperatures were all at 80 °C. The anode input H_2 and the cathode input O_2 flow rates were same. Two sets of *i*–*V* curves were obtained, one with H_2/O_2 flow rates of 200 mL min^{-1} and the other with H_2/O_2 flow rates of 700 mL min^{-1}.

Table 2
PEMFC performances data at H_2/O_2 flow rates = 200 mL min^{-1}.

MEA#	OCV (V)	PD_{max} (mW cm^2)	*Rs* (Ω cm^2)	*Rc* (Ω cm^2)
1	0.953	547	0.137 ± 0.002	0.241 ± 0.002
2	0.948	595	0.133 ± 0.001	0.235 ± 0.002
3	0.979 ± 0.013	614 ± 5	0.132 ± 0.001	0.194 ± 0.003
4	0.971	611	0.132 ± 0.001	0.206 ± 0.001
5	0.961	612	0.135 ± 0.002	0.241 ± 0.003
6	0.963 ± 0.011	626 ± 8	0.133 ± 0.001	0.206 ± 0.002
7	0.965	618	0.135 ± 0.002	0.206 ± 0.002
8	0.955	563	0.134 ± 0.001	0.240 ± 0.002
9	0.955	603	0.133 ± 0.002	0.212 ± 0.002
10	0.973	594	0.135 ± 0.002	0.224 ± 0.003
11	0.957	417	0.135 ± 0.001	0.267 ± 0.002
12	0.952	547	0.132 ± 0.002	0.247 ± 0.002
13	0.975	565	0.134 ± 0.002	0.230 ± 0.002

The cell was activated at 80 °C and at a constant voltage of 0.6 V for 30 min, then at open circuit for 3 min, and subsequently at a constant voltage of 0.4 V for 30 min to enhance humidification and activation of MEA. The above activation procedure was repeated 6 times before each *i–V* curve measurement was carried out. *i–V* curves were obtained by measuring the current density *i* with step decrement of voltage by an interval of 0.05 V. The time was held 30 s for each measurement. The active cell area was 5 cm × 5 cm. The reproducibility of *i–V* curves of MEA-3 and MEA-6 was investigated by three measurements with H_2/O_2 flow rates of 200 mL min^{-1} at three different dates. The errors of OCV (open circuit voltage) and PD_{max} (maximum power density) measurements are listed in Table 2.

2.4. Impedances measurements

The impedances of MEAs were measured at the same fuel cell test station as described in Section 2.3. The frequency response analyzer was a Model 850C Compact Fuel Cell Test Station (Scribner Associates, Inc.) and the potential state was kept at $i = 800$ mA cm^{-2}. The scanning frequency was from 10^4 Hz to 0.1 Hz. The active cell area was 5 cm × 5 cm.

2.5. 300 h continuous unit cell performance test

The performance of unit cell was tested at 80 °C and ambient pressure with a constant loading current ($i = 600$ mA cm^{-2}) using the same fuel cell testing instrument as described in Section 2.3. The area of testing fixture was 5 cm × 5 cm. The anode H_2 and cathode O_2 input flow rates were 200 mL min^{-1}. The voltage at the loading current ($i = 600$ mA cm^{-2}) was recorded every 30 s. The *i–V* polarization curve and AC-impedance measurements were carried out every 30 h. The *i–V* curves were obtained by measuring the current density *i* with step decrement of voltage by an interval of 0.05 V. The time was held 30 s for each measurement. The AC-impedance measurements were carried out at $i = 800$ mA cm^{-2}.

2.6. Morphology characterization of MEA

The catalyst layers morphology of MEA-1, -3, -6, and -9 after PEMFC tests under a H_2/O_2 flow rate of 200 mL min^{-1} and then a H_2/O_2 flow rate of 700 mL min^{-1} were examined using a scanning electron microscope (SEM, JEOL, JSM-6701F) and an energy dispersion spectroscopy (EDS, JEOL, JSM-6701F).

3. Results and discussion

3.1. Fuel cell tests of high Pt loading MEAs with H_2 and O_2 flow rates of 200 mL min^{-1}

In the first part of this study, the MEA-1–MEA-10 consisting of high Pt loadings (i.e. 0.5 mg cm^{-2} Pt at anode and 1.0 mg cm^{-2} Pt at cathode) were used for PEMFC tests. The H_2 and O_2 flows were set at a lower flow rate, i.e. 200 mL min^{-1}. Under a lower fuel and oxidant gas flow rate, the influence of catalyst layer structure on the feasibility of O_2 gases to reach the cathode Pt catalysis sites can be easily observed. The *i–V* curves and impedances of structure-a, -b, -c, and -d MEAs were investigated.

3.1.1. PEMFC performances of structure-b and structure-a MEAs

In this section, the PEMFC performances of structure-b MEA-2, -3, and -4 (the Pt-C-80 layer located at the interface between PEM and Pt-C-40 layer, Table 1) were investigated and compared with that of conventional structure-a MEA-1 (with only Pt-C-40 in the catalyst layer). Fig. 2 shows the *i–V* curves of MEA-1–MEA-4. These data show that at low current density, $i < 100$ mA cm^{-2},

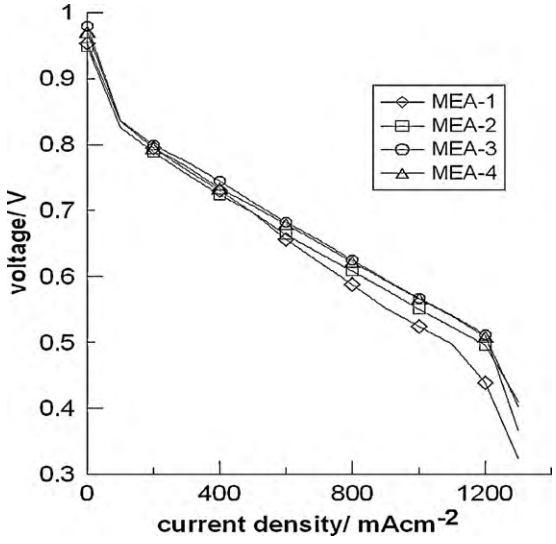

Fig. 2. PEMFC single cell test *i–V* curves at 80 °C and ambient pressure for MEA-1, -2, -3, and -4. H_2/O_2 flow rates were 200 mL min^{-1} with 100% RH. (◊) MEA-1; (□) MEA-2; (○) MEA-3; (△) MEA-4.

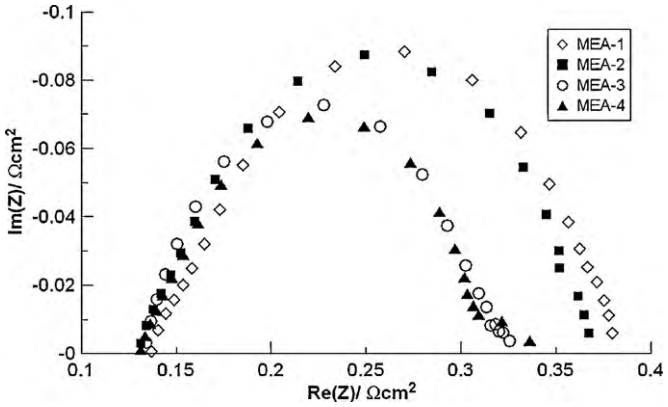

Fig. 3. Impedance spectra of H_2/O_2 PEMFC for MEA-1, -2, and -4 at 80 °C with an ambient pressure. The measurements were carried out at $i = 800$ mA cm^{-2}. H_2/O_2 flow rates were 200 mL min^{-1} with 100% RH. (◊) MEA-1; (■) MEA-2; (○) MEA-3; (▲) MEA-4.

the four MEAs had similar voltages. However as *i* was increased above 200 mA cm^{-2}, MEAs-2, -3, and -4 had higher voltage than MEA-1. The open circuit voltage (OCV) and maximum power density (PD_{max}) data of these MEAs are listed in Table 2. The data of Fig. 2 and Table 2 showed the fuel cell performance increased in the sequence of MEA-1 < MEA-2 < MEA-4 ≤ MEA-3. Fig. 3 shows the impedance spectra of MEA-1–MEA-4 obtained at a current density $i = 800$ mA cm^{-2}. The impedance spectra were fitted using an equivalent Randles circuit model as shown in Fig. 4 [22]. In Fig. 4, *Rs* represents the uncompensated ohmic resistance of electrochemical/electrical circuit and $Rs = R_{PEM} + R_{bulk+contact}$ (where R_{PEM} is the resistance of PEM and $R_{bulk+contact}$ the sum of the electri-

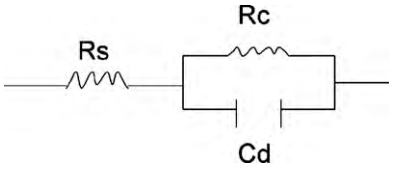

Fig. 4. Randles equivalent circuit of electrochemical half cells, composed of a resistor *Rs* in series with a resistor *Rc* and capacitor *Cd* [22].

cal circuit bulk resistance and contact resistance), *Rc* represents charge transfer resistance at the electrolyte/electrode interface in the catalyst layer, and *Cd* represents the double-layer capacitance at the electrolyte/electrode interface. Usually in a unit fuel cell $R_{bulk+contact} \ll R_{PEM}$ and the major contribution to *Rs* comes from the resistance of PEM, i.e. $Rs \simeq R_{PEM}$. The simulated *Rs* and *Rc* data and the errors are also summarized in Table 2. Table 2 shows these MEAs had similar *Rs* data, indicating similar ohmic resistance of these four MEAs. The reason for the similar *Rs* values of these four MEAs was because that same PEM, i.e. Nafion-212, was used in MEA preparations. However Fig. 3 and Table 2 show that MEA-2 had a slightly lower *Rc* value than MEA-1, and MEA-3 and MEA-4 had much lower *Rc* values than MEA-1. These results suggest that structure-b MEAs which were prepared by replacing 10–40 wt% of Pt-C-40 of the conventional structure-a MEA with Pt-C-80 had a lower charge transfer resistance in the catalyst layer. Since all of the four MEAs had same anode and cathode Pt loadings, the structure-b MEAs consisting of higher content of Pt-C-80 near the PEM should have lower content of large sizes carbon powders. Thus MEA-2, -3, and -4 had thinner catalyst layer thickness and more Pt catalysts locating near PEM than MEA-1. When a PEMFC is operated, the protons produced on the anode catalysis sites transfer from the anode catalysis sites through anode catalyst layer and PEM to the cathode catalysis sites. The structure-b MEA-2, -3, and -4 with a Pt-C-80 layer locating near PEM and thinner catalyst layers should have shorter proton transport path length in the catalyst layer. Thus MEA-2, -3, and -4 have lower *Rc* values than MEA-1. However, the data of Fig. 2 shows that MEA-4 had a slightly lower fuel cell performance than MEA-3, and also Fig. 3 and Table 2 show that MEA-4 had slight higher *Rc* than MEA-3. These results suggest that there is an optimum [Pt-C-80]/[Pt-C-40] wt ratio for a MEA to have a highest output power under a fixed Pt loading. Under a fixed Pt loading, raising the content of Pt-C-80 above the optimum [Pt-C-80]/[Pt-C-40] wt ratio in structure-b MEA could result in: (1) highly reduction of Pt catalysis surface area due to lots of large sizes Pt particles used in the electro-catalysis reaction and (2) highly reduction of the contact frequencies O_2 molecules with cathode Pt catalyst particles due to large amount of high Pt content Pt-C-80 catalysts locating near PEM. Since GDL is the inlet for H_2/O_2 gases to flow into anode and cathode, in cathode the catalysts locating near PEM which is far from GDL should have lower possibility for contacting O_2 molecules than those locating near GDL. Thus MEA-4 had a slight lower fuel cell performance and slight higher *Rc* than MEA-3.

3.1.2. PEMFC performances of structure-c and structure-a MEAs

In this section, the PEMFC performances of structure-c MEA-5, -6, and -7 (the Pt-C-80 layer located at the interface between Pt-C-40 layer and GDL, Table 1) were investigated and compared with that of structure-a MEA-1. Fig. 5 shows the *i–V* curves of MEA-1 and MEA-5–MEA-7 and The OCV and PD_{max} data obtained from Fig. 5 are summarized in Table 2. Fig. 5 shows that at low current density $i < 300\ mA\ cm^{-2}$, the four MEAs had almost same voltage. However as *i* was increased above $300\ mA\ cm^{-2}$, MEA-5, -6, and -7 had higher voltage than MEA-1. The impedance spectra of MEA-5–MEA-7 were also measured at $i = 800\ mA\ cm^{-2}$ and the simulated *Rs* and *Rc* data are summarized in Table 2. Table 2 shows the *Rs* values of MEA-5–MEA-7 were similar to those of MEA-1–MEA-4. The similar *Rs* values of these MEAs can also be attributed to the same PEM used in MEA preparations. Table 2 also shows that MEA-5 had a *Rc* value similar to MEA-1, but a higher output power than MEA-1. The MEA-5 was prepared by replacing 10 wt% of Pt-C-40 of structure-a MEA-1 with Pt-C-80 and coating the Pt-C-80 at the interface between Pt-C-40 and GDL. Though the replacement of Pt-C-40 with Pt-C-80 resulted in a lower thickness of catalyst layer. The resistance of proton transport in the catalyst layer is proportional

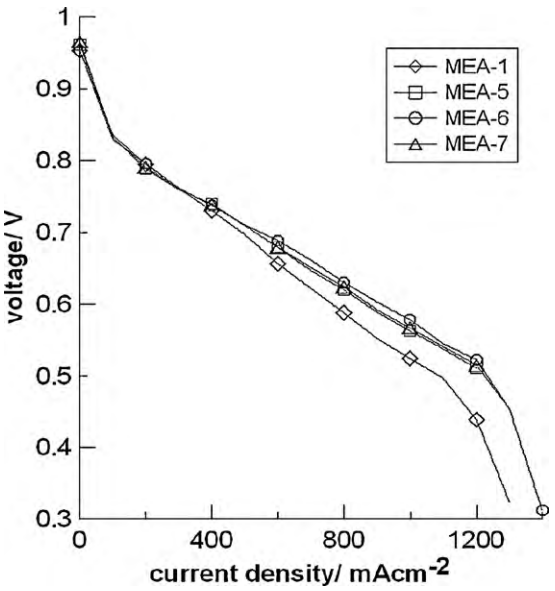

Fig. 5. PEMFC single cell test *i–V* curves at 80 °C and ambient pressure for MEA-1 and MEA-5, -6, and -7. H_2/O_2 flow rates were 200 mL min^{-1} with 100% RH. (◊) MEA-1; (□) MEA-5; (○) MEA-6; (△) MEA-7.

to its transportation length. The lower thickness of catalyst layer could result in a lower resistance of catalyst layer. Since all the Pt-C-80 particles were located near the GDL and far from PEM, the decrement of proton transport resistance due to lower thickness of catalyst layer was compensated by the longer distance from the location of Pt-C-80 particles (near the interface of catalyst layer and GDL) to PEM. Thus MEA-5 had a *Rc* value similar to the *Rc* of MEA-1. The higher output power of MEA-5 than MEA-1 can be attributed to the higher feasibility O_2 gases to reach Pt catalysis particles at cathode, because of more Pt particles locating near GDL (the inlet of H_2/O_2 gases into MEA).

Table 2 shows at a fixed Pt loading, the structure-c MEAs have *Rc* values higher than structure-b MEAs, because of more high Pt content Pt-C-80 particles locating near GDL. The Pt particles locating near GDL are far from PEM and have longer proton transport path length than those locating near PEM. Table 2 also shows that MEA-6 and MEA-7 had lower *Rc* values than MEA-1 and MEA-5. These results suggest that replacing 20–40 wt% of Pt-C-40 in catalyst layer of structure-a MEA-1 with Pt-C-80 and coating the Pt-C-80 particles at the interface of Pt-C-40 and GDL result in a reduction of proton transport resistance in catalyst layer. Because of more Pt-C-80 particles located near GDL in MEA-6 and MEA-7, the distance between GDL and PEM was shorter and the transport resistance of protons produced from Pt-C-80 particles was lower in MEA-6 and MEA-7 than in MEA-1 and MEA-5. Fig. 5 and Table 2 show that MEA-6 and MEA-7 had a higher fuel cell performance than MEA-1 and MEA-5. The higher fuel cell performances of MEA-6 and MEA-7 can be attributed to its lower *Rc* and higher feasibility for O_2 gases to reach cathode Pt particles, because of more high Pt content Pt-C-80 particles located near GDL. Similar to structure-b MEA, there is an optimum [Pt-C-80]/[Pt-C-40] wt ratio for structure-c MEAs to have a highest output power under a fixed Pt loading. In the present work, MEA-6 showed its catalyst layer had an optimum [Pt-C-80]/[Pt-C-40] wt ratio in structure-c MEAs. Raising Pt-C-80 loading above the optimum [Pt-C-80]/[Pt-C-40] wt ratio in structure-c MEA (i.e. MEA-7) caused a lowering of Pt catalysis surface area due to the replacement of large quantity of Pt-C-40 with Pt-C-80. Thus MEA-7 had a slightly lower output power than MEA-6.

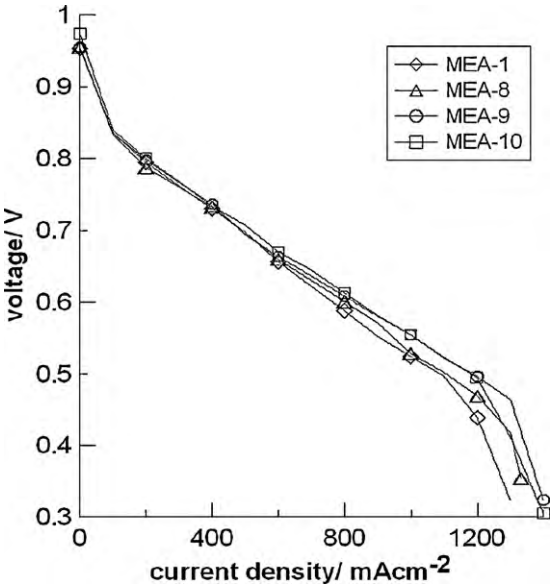

Fig. 6. PEMFC single cell test *i–V* curves at 80 °C and ambient pressure for MEA-1 and MEA-8, -9, and -10. H_2/O_2 flow rates were 200 mL min^{-1} with 100% RH. (◊) MEA-1; (△) MEA-8; (○) MEA-9; (□) MEA-10.

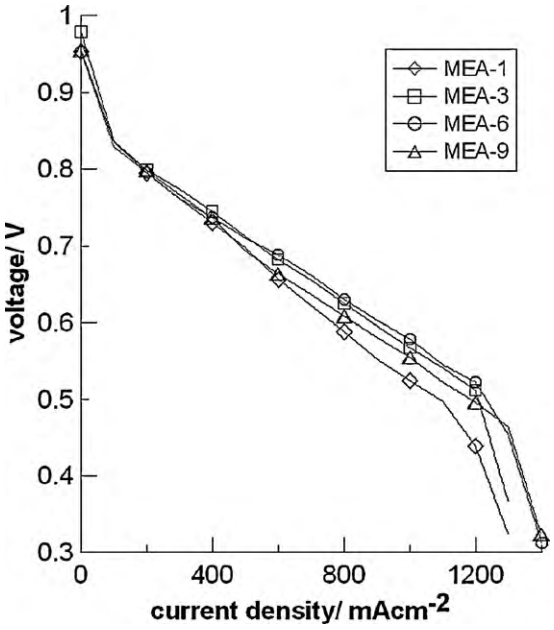

Fig. 7. PEMFC single cell test *i–V* curves at 80 °C and ambient pressure for MEA-1 and MEA-3, -6, and -9. H_2/O_2 flow rates were 200 mL min^{-1} with 100% RH. (◊) MEA-1; (□) MEA-3; (○) MEA-6; (△) MEA-9.

3.1.3. PEMFC performances of structure-d and structure-a MEAs

In this section, the PEMFC performances and impedances of structure-d MEA-8, -9, and -10 (Pt-C-40 and Pt-C-80 were homogeneously mixed in the catalyst layer, Table 1) were investigated and compared with that of structure-a MEA-1. Fig. 6 shows the *i–V* curves of MEA-1 and MEA-8–MEA-10. The OCV and PD_{max} data obtained from Fig. 6 and the simulated *Rs* and *Rc* data obtained at $i = 800$ mA cm^{-2} are also summarized in Table 2. Fig. 6 shows that at low current density $i < 400$ mA cm^{-2}, these four MEAs had almost same voltage. However as *i* was increased above 400 mA cm^{-2}, MEA-8, MEA-9, and MEA-10 had voltages higher than MEA-1. Table 2 also shows the *Rs* values of MEA-8–MEA-10 were similar to those of MEA-1–MEA-7, due to the same PEM used in the MEA preparations. Table 2 shows that MEA-8 had a *Rc* value similar to that of MEA-1 and MEA-9 and MEA-10 had *Rc* values lower than MEA-1. These results suggest that structure-d MEA-9 and MEA-10 which were prepared by replacing 10–20 wt% of Pt-C-40 of structure-a MEA-1 with Pt-C-80 had lower proton transfer resistance in the catalyst layers than MEA-1. Similar to structure-b and structure-c MEAs, the reason of lower *Rc* values of MEA-9 and MEA-10 than MEA-1 can be attributed to the thinner catalyst layer thickness of MEA-9 and MEA-10 than MEA-1. Fig. 6 and Table 2 also show that MEA-9 and MEA-10 had better fuel cell performance than MEA-1 and MEA-8. The better fuel cell performance of MEA-9 and MEA-10 than MEA-1 and MEA-8 can also be attributed to the lower *Rc* and higher feasibility for O_2 gases to reach cathode Pt particles in MEA-9 and MEA-10 than in MEA-1 and MEA-8. Because of more Pt-C-80 particles and less Pt-C-40 particles were mixed in the catalyst layer, MEA-9 and MEA-10 had lower catalyst layer thickness and more Pt particles locating near GDL than MEA-1 and MEA-8. Thus MEA-9 and MEA-10 had lower *Rc* values and higher efficiency for O_2 molecules to reach cathode Pt catalyst particles. Similar to structure-b and –c MEAs, there is an optimum [Pt-C-80]/[Pt-C-40] wt ratio for a structure-d MEA to have a highest output power under a fixed Pt loading. In the present work, MEA-9 showed its catalyst layer had an optimum [Pt-C-80]/[Pt-C-40] wt ratio in structure-d MEAs. Raising Pt-C-80 loading above the optimum [Pt-C-80]/[Pt-C-40] wt ratio (i.e. MEA-10) caused a lowering of Pt catalysis surface area due to the replacement of large quantity of Pt-C-40 with Pt-C-80. Thus MEA-10 had an output power similar to MEA-9.

3.1.4. Comparison of PEMFC performances of structure-a, -b, -c, and -d MEAs

In this section, we compare the fuel cell performances of structure-a MEA-1, structure-b MEA-3, structure-c MEA-6, and structure-d MEA-9. The MEA-3, MEA-6, and MEA-9 had same Pt-C-80 and Pt-C-40 catalysts loadings. The differences between these three MEAs were the locations of Pt-C-80 and Pt-C-40 catalyst layers as shown in Fig. 1. Fig. 7 shows the PEMFC *i–V* curves of these four MEAs. From Fig. 7, we found that at $i < 200$ mA cm^{-2} the voltages of these MEAs were very close. However at $i > 500$ mA cm^{-2}, the *i–V* curves show at a fixed *i* value the voltages of these MEAs decreases in the sequence of MEA-6 > ∼MEA-3 > MEA-9 > MEA-1. Table 2 shows the *Rc* value increases in the sequence of MEA-3 < MEA-6 < MEA-9 < MEA-1, indicating the resistance of catalyst layers increases in the sequence of MEA-3 < MEA-6 < MEA-9 < MEA-1. Since the high Pt content Pt-C-80 layer located near PEM in structure-b MEA (Fig. 1b) and the Pt-C-80 layer located near GDL in structure-c MEA (Fig. 1c), the protons produced on the Pt particles surfaces of Pt-C-80 in structure-b MEA had shorter transport path length than those in structure-c MEA. Thus more protons produced in cathode of MEA-3 have shorter transport path length than in MEA-6, and MEA-3 has a lower *Rc* than MEA-6. As shown in Table 2, MEA-3, MEA-6, and MEA-9 consist of same quantities of Pt-C-40 and Pt-C-80, indicating these three MEAs have same Pt particles catalysis surface area. The behavior of better fuel cell performance of structure-b MEA-3 than structure-d MEA-9 at $i > 500$ mA cm^{-2} could be due to the lower *Rc* of MEA-3 than MEA-9. The phenomenon of structure-c MEA-6 having higher voltage at $i > 500$ mA cm^{-2} than structure-b MEA-3 and structure-d MEA-9 can be attributed to the better feasibility of O_2 gas molecules to reach the cathode Pt catalyst particles of MEA-c, in which the high Pt content Pt-C-80 particles locate near GDL, i.e. the inlet of H_2/O_2 gases into catalyst layers, and easy for O_2 molecules to reach cathode Pt particles. In the following sections, we will increase the H_2/O_2 flow rates to 700 mL min^{-1} and investigate the performances of MEAs consisting of various catalyst layer structures. Increasing H_2/O_2 flow rates increases the chance for Pt particles to catch H_2/O_2 molecules. The comparison of the fuel cell performance of PEMFCs operated at a H_2/O_2 flow rate of 200 mL min^{-1} with those oper-

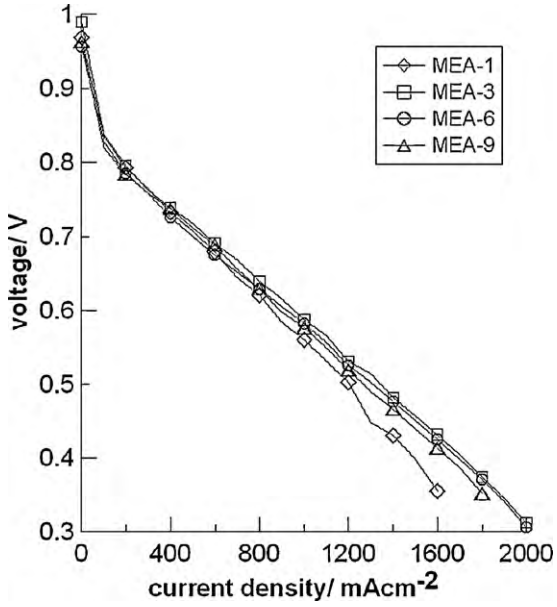

Fig. 8. PEMFC single cell test *i–V* curves at 80 °C and ambient pressure for MEA-1 and MEA-3, -6, and -9. H_2/O_2 flow rates were 700 mL min^{-1} with 100% RH. (◊) MEA-1; (□) MEA-3; (○) MEA-6; (△) MEA-9.

ated at a H_2/O_2 flow rate of 700 mL min^{-1} allow us to have a better understanding on the influence of the MEA catalyst layer structure on "*the feasibility for O_2 gases to reach cathode Pt catalyst particles*", and thus on the fuel cell performance of a PEMFC.

3.2. Fuel cell tests of high Pt loading MEAs with H_2 and O_2 flow rates of 700 mL min^{-1}

As we mentioned before, the proton transport resistance in the catalyst layers and the contact frequency of O_2 molecules with cathode catalysts particles are the key factors controlling the fuel cell performance. When the H_2/O_2 flows were set at a low flow rate, i.e. 200 mL min^{-1} with low H_2/O_2 reactants input, the factor "feasibility for O_2 molecules to reach cathode Pt catalyst particles" might be more important than the factor "proton transport resistance in catalyst layer" for controlling fuel cell performance. In this section, the H_2/O_2 flows were set at a high flow rate, i.e. 700 mL min^{-1}. The structure-a MEA-1, structure-b MEA-3, structure-c MEA-6, and structure-d MEA-9 which had same Pt-C-40 and Pt-C-80 loadings were used to investigate the PEMFC unit cell performance. The *i–V* curves and impedances of these MEAs were investigated. The main purpose of this work is to reduce the influence of the factor "feasibility of O_2 molecules to reach cathode Pt particles" on controlling fuel cell performance. With sufficient supply of H_2 and O_2 reactant molecules, "proton transport resistance in catalyst layer" may be more important than "contact frequency of O_2 molecules with cathode Pt particles" for controlling fuel cell performance.

Fig. 8 shows the PEMFC unit cell test *i–V* curves of MEA-1, MEA-3, MEA-6, and MEA-9 at 80 °C with 100% RH and at ambient pressure with H_2/O_2 flow rates of 700 mL min^{-1}. In Table 3, we summarize the unit cell *OCV* and PD_{max} data of these MEAs at a H_2/O_2 flow rate of 700 mL min^{-1}. Comparing the *i–V* curves of MEA-1, MEA-3, MEA-6, and MEA-9 shown in Fig. 8 with those shown in Fig. 7 and the PD_{max} data of MEA-1, MEA-3, MEA-6, and MEA-9 shown in Table 3 with those shown in Table 2, we found for a same MEA the fuel cell performance was improved when the H_2/O_2 flow rates were increased from 200 mL min^{-1} to 700 mL min^{-1}. The increment of output power can be attributed to the increments of e^- and H^+ generated in the electrochemical reaction by increasing H_2 and O_2 reactant concentrations in the fuel cell anode and cathode, respectively.

Table 3
PEMFC performances data at H_2/O_2 flow rates = 700 mL min^{-1}.

MEA#	OCV (V)	PD_{max} (mW cm^2)	*Rs* (Ω cm^2)	*Rc* (Ω cm^2)
1	0.968	603	0.137 ± 0.002	0.189 ± 0.001
3	0.989	691	0.137 ± 0.002	0.138 ± 0.002
6	0.965	681	0.140 ± 0.002	0.163 ± 0.002
9	0.963	662	0.130 ± 0.002	0.176 ± 0.001
11	0.961	546	0.137 ± 0.002	0.229 ± 0.002
12	0.985	673	0.131 ± 0.002	0.198 ± 0.002
13	0.962	668	0.134 ± 0.002	0.191 ± 0.002

The impedance measurements of MEA-1, MEA-3, MEA-6, and MEA-9 at i = 800 mA cm^{-2} were also carried out at 80 °C with 100% RH and at ambient pressure with H_2/O_2 flow rates of 700 mL min^{-1}. The simulated *Rs* and *Rc* data are also summarized in Table 3. Comparing the impedance data of Table 3 with those of Table 2, we found MEA-1, MEA-3, MEA-6, and MEA-9 had similar *Rs* values and the *Rs* value did not change significantly with H_2/O_2 flow rates, suggesting the proton transport resistance of a membrane was independent of H_2/O_2 flow rates. The reason for the independency of membrane *Rs* of H_2 and O_2 flow rates could be due to the same humidity (100% RH) of the input 200 mL min^{-1} H_2 flow and 700 mL min^{-1} H_2 flow. However, the impedance data showed all *Rc* values of these MEAs decreased when the H_2/O_2 flow rates were increased from 200 mL min^{-1} to 700 mL min^{-1}. Increasing H_2 and O_2 flow rates in anode and cathode, respectively, reduces the resistance caused from mass-transport process and thus a lowering of charge transfer resistance [23]. But the relative variations in *Rc* values among different MEAs did not change significantly when the H_2 and O_2 flow rates were increased from 200 mL min^{-1} to 700 mL min^{-1}, indicating influence of catalyst layer structure on *Rc* value is also independent of H_2 and O_2 flow rates.

The *i–V* curves of Fig. 8 and PD_{max} data of Table 3 show the performance of MEA-1 was worse than those of MEA-3, -6, and -9 when the H_2/O_2 input flow rates were set at 700 mL min^{-1}. This behavior is similar to the behavior of MEAs with H_2/O_2 input flow rates operated at 200 mL min^{-1} (Fig. 7 and Table 2). Table 3 shows the *Rc* value increased in the sequence of MEA-3 < MEA-6 < MEA-9 < MEA-1 when H_2/O_2 input flow rate was set at 700 mL min^{-1}, which was similar to the behavior of *Rc* values at a H_2/O_2 input flow rate of 200 mL min^{-1} as shown in Table 2, i.e. *Rc* value increased in the sequence of MEA-3 < MEA-6 < MEA-9 < MEA-1 at a H_2/O_2 input flow rate of 200 mL min^{-1}. Fig. 8 and Table 3 show at i > 400 mA cm^{-2}, the voltages of the fuel cells decreased in the sequence of MEA-3 > MEA-6 > MEA-9 > MEA-1 when H_2/O_2 input flow rate was set at 700 mL min^{-1}, which was different to the behavior of voltages at a H_2/O_2 input flow rate of 200 mL min^{-1}. Fig. 7 and Table 2 show the voltage at i > 400 mA cm^{-2} decreases in the sequence of MEA-6 > MEA-3 > MEA-9 > MEA-1 when H_2/O_2 input flow rate was set at 200 mL min^{-1}. These data show that at a low H_2/O_2 input flow rate (i.e. 200 mL min^{-1}) structure-c MEA-6 (Pt-C-80 layer was near GDL) had a better fuel cell performance than structure-b MEA-3 (Pt-C-80 layer was near PEM) and at a high H_2/O_2 input flow rate (i.e. 700 mL min^{-1}) structure-b MEA-3 had a better fuel cell performance than structure-c MEA-6. These results suggest that when the fuel cell was operated at a low H_2/O_2 input flow rate 200 mL min^{-1} the factor "*feasibility for O_2 molecules to reach cathode Pt particles*" is more important than the factor "*proton transport resistance in catalyst layers*" for controlling fuel cells performance. Locating high Pt content Pt-C-80 particles near GDL in structure-c MEA results in more Pt particles locating near GDL and favors O_2 molecules to reach cathode Pt particles. At a high H_2/O_2 input flow rate 700 mL min^{-1}, the factor "*feasibility for O_2 molecules to reach cathode Pt particles*" is less important than the factor "*proton*

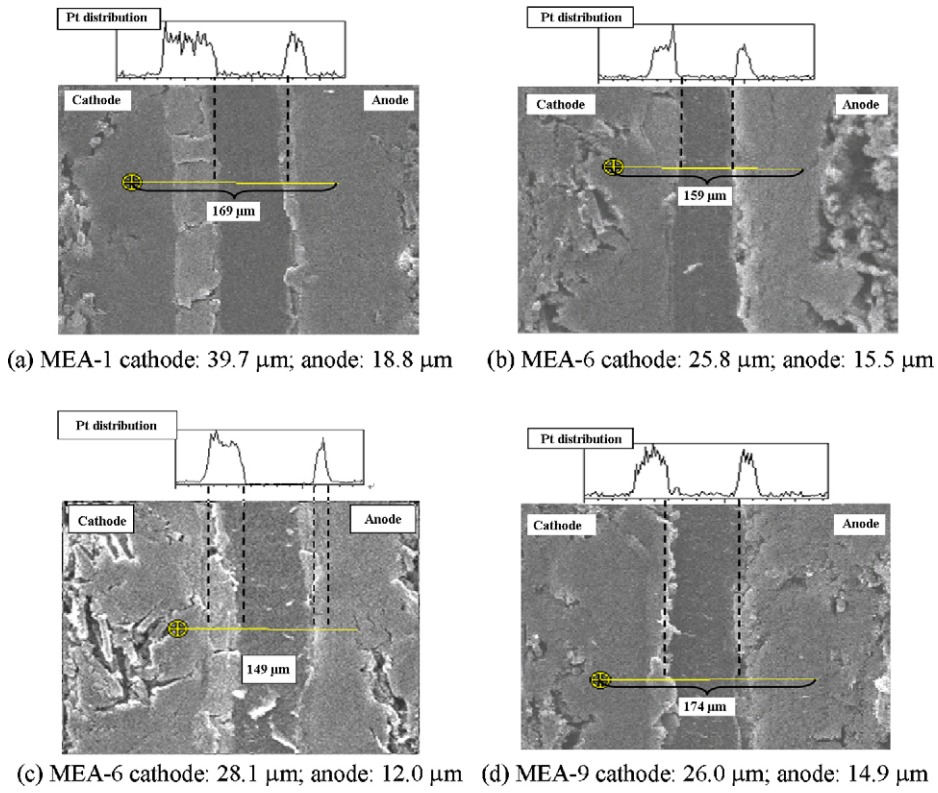

Fig. 9. SEM and EDS *Pt* distribution data along the MEA cross-section for MEAs after unit cell test with H_2/O_2 flow rates of 200 mL min^{-1} and 700 mL min^{-1}. The left side is cathode and right side is anode. (a) MEA-1; (b) MEA-3; (c) MEA-6; (d) MEA-9.

transport resistance in catalyst layers" for controlling fuel cell performance. Since the contact efficiency of O_2 molecules with cathode Pt particles is increased at a high H_2/O_2 input flow rate, "proton transport resistance in catalyst layers" should be the more important than "the contact efficiency of O_2 molecules with cathode Pt particles" for controlling fuel cell performance when the H_2/O_2 input gases are set at a high flow rate 700 mL min^{-1}. Thus at a H_2/O_2 input flow rate of 700 mL min^{-1}, structure-b MEA-3 had a better fuel cell performance than structure-c MEA-6.

3.3. SEM and EDS studies of structure-a, -b, -c, and -d MEAs

The cross-sections of MEA-1, -3, -6, and -9 after unit cell tests under H_2/O_2 flow rates of 200 mL min^{-1} and then under H_2/O_2 flow rates of 700 mL min^{-1} were investigated using SEM and EDS analyses. The SEM micrographs of the cross-sections of these MEAs and the EDS Pt element distributions along the direction from cathode to anode of the cross-sections of these MEAs are shown in Fig. 9. As shown in Fig. 9a and d, the Pt element distributed homogeneously in structure-a MEA-1 and structure-d MEA-9. Fig. 9b shows a higher Pt density distribution near PEM in structure-b MEA-3 and Fig. 9c shows a higher Pt density distribution near GDL. The thicknesses of cathode and anode Pt layers of these four MEAs obtained from Fig. 9 are summarized in Table 4. The data of Table 4 shows the Pt layers thicknesses of MEA-3, -6, and -9 are thinner than that of MEA-1.

Table 4
Thicknesses of cathode and anode catalyst layers of MEAs after unit cell tests with H_2/O_2 flow rates of 200 mL min^{-1} and then with H_2/O_2 flow rates of 700 mL min^{-1}.

MEA#	Cathode thickness (μm)	Anode thickness (μm)
1	39.7	18.8
3	26.0	15.5
6	28.1	12.0
9	26.0	14.9

These results indicated the structures of the MEAs prepared in lab were consistent with the MEA structure designs shown in Fig. 1.

3.4. Fuel cell tests of low Pt loading MEAs

As shown in previous sections, the PEMFC performance was improved using the modified structures -b, -c, and -d MEAs. As mentioned in Section 1, the high cost of Pt is one of the issues causing impediment to the commercialization of PEMFC. Thus the modified MEAs with low Pt content was prepared in this section to investigate the fuel cell performance. In present section, the anode and cathode Pt loadings of structures -a and -c MEAs were reduced to 0.3 mg cm^{-2} and 0.6 mg cm^{-2}, respectively. The catalyst compositions of these two MEAs are also listed in Table 1 and designated as MEA-11 (structure-a) and MEA-12 (structure-c). Another issue is the different diffusivity of H_2 and O_2 molecules in anode and cathode, respectively, is considered in this section. It is the much lower diffusivity of O_2 molecules in cathode causes the diffusion limitation of reactant gas molecules in catalyst layers. Thus another MEA-13 (designated as structure-ac) consisting same anode catalyst layer structure as that of structure-a MEA-11 and same cathode catalyst layer structure as that of structure-c MEA-12 was prepared. The catalyst composition of MEA-13 is also listed in Table 1.

Figs. 10 and 11 show the unit cell test *i–V* curves and impedance spectra at $i = 800$ mA cm^{-2}, respectively, of MEA-11, MEA-12, and MEA-13 at 80 °C with H_2/O_2 flow rates of 200 mL min^{-1} and 100% RH. Similar *i–V* curves and impedance spectra measurements of MEA-11, MEA-12, and MEA-13 were also carried out with H_2/O_2 flow rates of 700 mL min^{-1} and 100% RH and the *i–V* curves are shown in Fig. 12. The OCV, PD_{max}, *Rs*, and *Rc* data of these MEAs are also summarized in Tables 2 and 3 for H_2/O_2 flow rates of 200 mL min^{-1} and 700 mL min^{-1}, respectively.

Figs. 10 and 12 show that at low current density $i < 300$ mA cm^{-2}, these three MEAs had almost the same voltage. However as *i* was

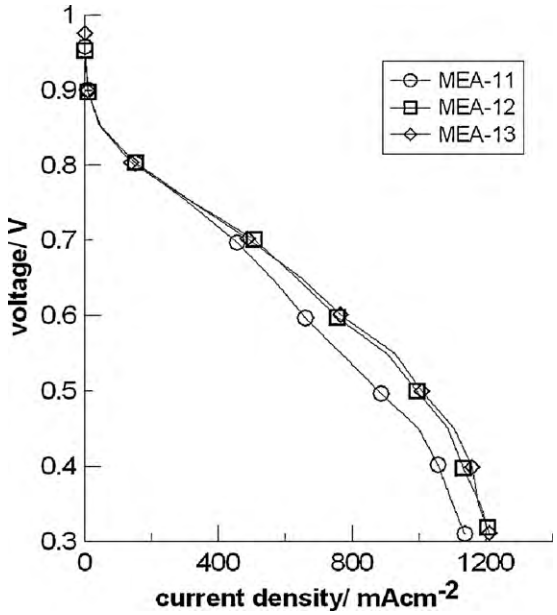

Fig. 10. PEMFC single cell test *i–V* curves at 80 °C and ambient pressure for MEA-11, MEA-12, and MEA-13. H_2/O_2 flow rates were 200 mL min^{-1} with 100% RH. (○) MEA-11; (□) MEA-12; (◊) MEA-13.

increased above 300 mA cm^{-2}, the voltages of MEA-12 and -13 were similar, but higher than that of MEA-11. Tables 2 and 3 show these three MEAs had similar OCV values, however, the PD_{max} data of MEA-12 and MEA-13 were higher than that of MEA-11. Tables 2 and 3 show that MEA-11, MEA-12 and MEA-13 had similar *Rs* values. The similar *Rs* values of these MEAs can also be attributed to the same PEM used in MEA preparations. Tables 2 and 3 also show that MEA-12 and MEA-13 had similar *Rc* values, but lower *Rc* values than MEA-11. These results suggest the modified structure-c and structure-ac MEAs had better fuel cell performance than structure-a MEA when the Pt catalyst loading was lowered. The behavior of similar fuel cell performances of MEA-12 (structure-c: both anode and cathode catalyst layers were c-structure) with MEA-13 (structure-ac: the anode catalyst layer was a-structure and the cathode catalyst layer was c-structure) suggests that diffusion of O_2 molecules in cathode is the main limitation of the diffusion of reactant gases diffusing in catalyst layers.

Comparing the fuel cell performance and impedance data of MEA-11 (structure-a) with those of MEA-1 (structure-a) and fuel cell performance and impedance data of MEA-12 (structure-c) and

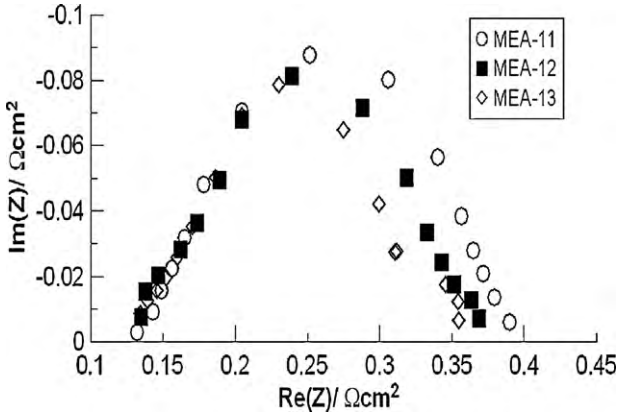

Fig. 11. Impedance spectra of H_2/O_2 PEMFC for MEA-11, MEA-12, and MEA-13 at 80 °C with 100% RH. The measurements were carried out at i = 800 mA cm^{-2}. H_2/O_2 flow rates were 200 mL min^{-1}. (○) MEA-11; (■) MEA-12; (◊) MEA-13.

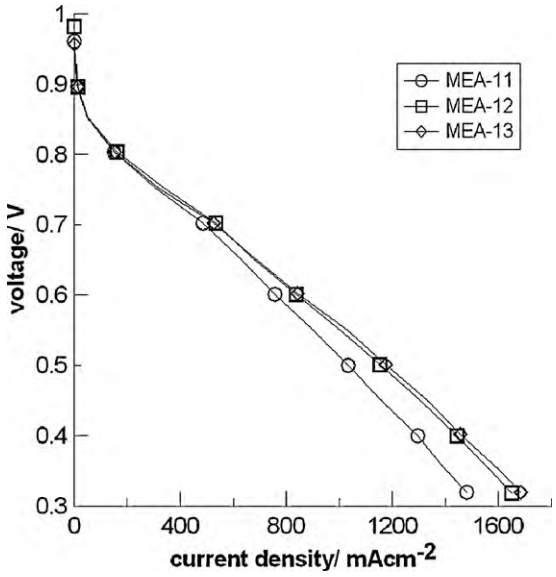

Fig. 12. PEMFC single cell test *i–V* curves at 80 °C and ambient pressure for MEA-11, MEA-12, and MEA-13. H_2/O_2 flow rates were 700 mL min^{-1} with 100% RH. (○) MEA-11; (□) MEA-12; (◊) MEA-13.

MEA-13 (structure-ac) with those of MEA-6 (structure-c), we found for MEAs with similar catalyst layer structure the fuel cell performances were lowered and Rc values were raised when the Pt loadings were reduced (Figs. 7, 8, 10 and 12, and Tables 2 and 3). Similar results were also reported by Paganin et al. [24]. It was explained high catalyst loading leads the electrode to have a higher catalysis surface area and less charge transfer resistance and thus a higher fuel cell performance [23].

From the data of Figs. 7, 8, 10 and 12 and Tables 2 and 3, we also found the fuel cell performances of structure-c MEA-12 and structure-ac MEA-13 were similar to that of structure-a MEA-1. These results suggest by using the modified structure-a and structure-ac MEAs the Pt loadings can be lowered to 60% of the Pt loading of the conventional structure-a MEA (with cathode and anode Pt loadings of 1.0 mg cm^{-2} and 0.5 mg cm^{-2}, respectively) without losing fuel cell performance. Further decreasing of Pt load-

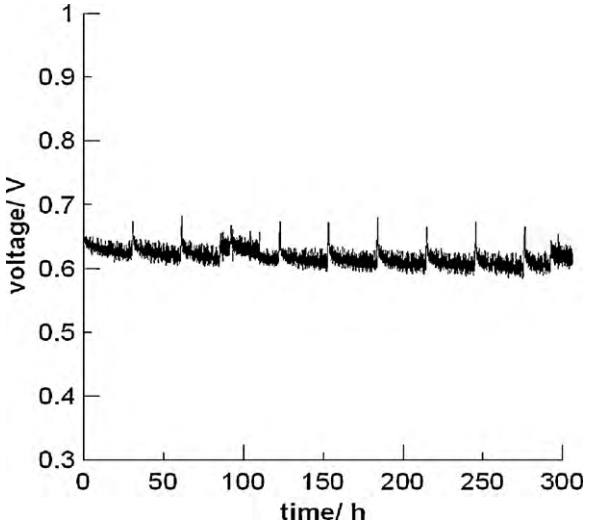

Fig. 13. The variation of voltage of the unit cell of MEA-12 under 300 h continuous operation at 80 °C with a constant current density i = 600 mA cm^{-2}. H_2/O_2 flow rates were 200 mL min^{-1} with 100% RH. The *i–V* curve (Fig. 14) and impedance (Fig. 15) measurements were carried out every 30 h. The voltage versus time curve shows fluctuation every 30 h.

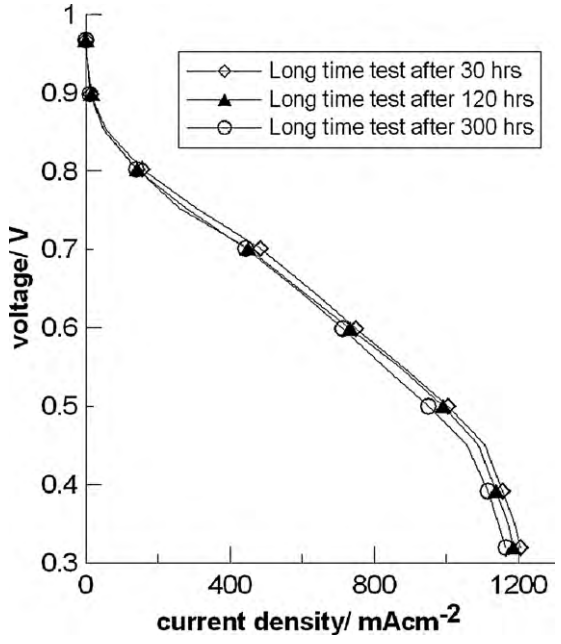

Fig. 14. The *i*–*V* curves of the unit cell of MEA-12 obtained at (◊) 30 h, (▲) 120 h, and (○) 300 h during 300 h continuous operation at 80 °C with a constant current density $i = 600\ mA\ cm^{-2}$. H_2/O_2 flow rates were $200\ mL\ min^{-1}$ with 100% RH.

ing causes a further reduction of catalyst layer thickness and a lower dependency of fuel cell performance on the O_2 diffusion at cathode and proton transport resistance in catalyst layer. Thus the fuel cell performance is mainly controlled by catalysis activity of catalysts particles. Structure-a MEA consisting only of Pt-C-40 catalysts could have better fuel cell performance than structure-b, -c, and -d MEAs consisting of Pt-C-40 and Pt-C-80 catalysts. This topic will be our future research project.

3.5. Durability of structure-c MEA

The durability of MEA-12 (structure-c) was investigated by operating the unit cell at 80 °C with a constant $i = 600\ mA\ cm^{-2}$ and H_2/O_2 flow rates of $200\ mL\ min^{-1}$. Fig. 13 shows the variation of voltage versus operating time for 300 h continuous operation. Since *i*–*V* polarization curve and AC-impedance measurements were carried out every 30 h. Fig. 13 shows fluctuation of voltage for every 30 h of operation. These data indicate an average voltage decay of $9.3 \times 10^{-5}\ V\ h^{-1}$. Figs. 14 and 15 are the *i*–*V* curves and impedance spectra at $i = 800\ mA\ cm^{-2}$, respectively, obtained at 30 h, 120 h, and 300 h operating times. These results showed no significant changes in *i*–*V* and impedance data at these three operating times, suggesting low MEA decay during the 300 h continuous operation.

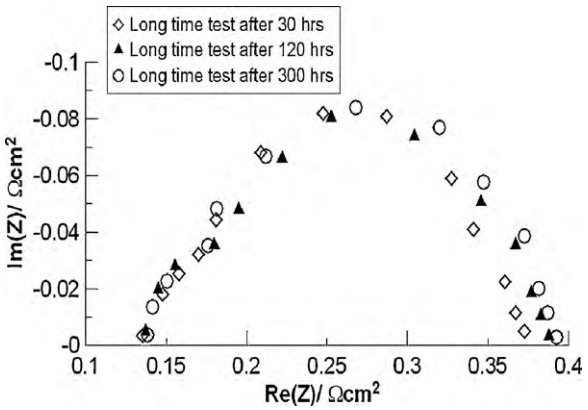

Fig. 15. The impedances of the unit cell of MEA-12 obtained at (◊) 30 h; (▲) 120 h; and (○) 300 h during 300 h continuous operation at 80 °C with a constant current density $i = 800\ mA\ cm^{-2}$. H_2/O_2 flow rates were $200\ mL\ min^{-1}$ with 100% RH.

4. Conclusions

In this work we showed that under a fixed Pt loading, the modified 7-layer and 9-layer MEAs with 20–40 wt% of Pt catalyst contributed from Pt-C-80 and 80–60 wt% of Pt catalyst contributed from Pt-C-40 and coating the thin Pt-C-80 layer either at the interface between Pt-C-40 layer and PEM (structure-b MEA) or/and at the interface between Pt-C-40 layer and GDL (structure-c MEA/and structure-d MEA) had better fuel cell performances than the conventional structure-a MEA with 100 wt% Pt catalyst contributed from Pt-C-40. The replacement of Pt-C-40 with Pt-C-80 causes a reduction of the content of large sizes carbon support powders and thus the thickness of catalyst layers. The lower thickness of catalyst layer results in a lower proton transport resistance in catalyst layers and a higher efficiency for the O_2 molecules to reach cathode Pt electro-catalytic sites, particularly when the fuel cell is operated at a high current. The replacement of 20–40 wt% of Pt-C-40 (Pt particles specific surface area $100\ m^2\ g^{-1}$) with Pt-C-80 (Pt particle specific surface area $57\ m^2\ g^{-1}$) causes a little loss of Pt particles surface area and thus the Pt catalysis activity. The loss of Pt catalysis activity can be overcome by the reduction of proton transport resistance and the improvement of the efficiency for O_2 molecules to reach the Pt electro-catalytic sites. Thus the modified structure-b, -c, and -d MEAs had better fuel cell performance than the conventional structure-a MEA. The data also showed that for MEAs with same Pt-C-40 and Pt-C-80 catalysts loadings, structure-c MEA (Pt-C-80 layer was near GDL) had a better fuel cell performance than structure-b MEA (Pt-C-80 layer was near PEM) when H_2/O_2 was operated at a low flow rate (i.e. $200\ mL\ min^{-1}$) and structure-b had a better fuel cell performance than structure-c when H_2/O_2 was operated at a high flow rate (i.e. $700\ mL\ min^{-1}$). These results suggest that at a low H_2/O_2 input flow rate $200\ mL\ min^{-1}$ the factor "*feasibility for O_2 molecules to reach cathode Pt particles*" is more important than the factor "*proton transport resistance in catalyst layers*" for controlling fuel cells performance. The structure-c MEA with high Pt content Pt-C-80 particles located near GDL (i.e. the inlet of H_2/O_2 to catalysis sites) favoring *O_2 molecules to reach cathode Pt particles* had a better fuel cell performance than structure-b MEA at a low H_2/O_2 flow rate. At a high H_2/O_2 input flow rate $700\ mL\ min^{-1}$, the factor "*feasibility for O_2 molecules to reach cathode Pt particles*" is less important than the factor "*proton transport resistance in catalyst layers*" for controlling fuel cell performance, since the contact efficiency of H_2/O_2 molecules with Pt particles is increased at a higher H_2/O_2 input flow rate. The structure-b MEA consisting of high Pt content Pt-C-80 located near PEM had a lower proton transport resistance in catalyst layer than structure-c MEA consisting of high Pt content Pt-C-80 located near GDL. Thus at a higher H_2/O_2 input flow rate, structure-b MEA had a better fuel cell performance structure-c MEA.

Acknowledgement

The authors would like to thank for the financial support by Ministry of Economic Affairs of Taiwan ROC (98-D0204-4).

References

[1] M. Watanabe, in: W. Vielstich, A. Lamm, H.A. Gasteiger (Eds.), Handbook of Fuel Cells, vol. 2, 2003 (Chapter 28);
A. Lasita, in: W. Vielstich, A. Lamm, H.A. Gasteiger (Eds.), Handbook of Fuel Cells, vol. 2, 2003 (Chapter 29);

S. Mukerjee, S. Srinivasan, in: W. Vielstich, A. Lamm, H.A. Gasteiger (Eds.), Handbook of Fuel Cells, vol. 2, 2003 (Chapter 34).
[2] V. Mehta, J.S. Cooper, J. Power Sources 114 (2003) 32–53.
[3] S.D. Thompson, L.R. Jordan, M. Forsyth, Electrochim. Acta 46 (2001) 1657–1663.
[4] Q. Wang, M. Eikerling, D. Song, Z. Liu, T. Navessin, Z. Xie, S. Holdcroft, J. Electrochem. Soc. 151 (7) (2004) A950–957.
[5] Z. Xie, T. Navessin, K. Shi, R. Chow, Q. Wang, D. Song, B. Audreaus, M. Eikerling, Z. Liu, S. Holdcroft, J. Electrochem. Soc. 152 (6) (2005) A1171–1179.
[6] M.S. Wilson, S. Gottesfeld, J. Electrochem. Soc. 139 (1992) L28–30.
[7] M.S. Wilson, S. Gottesfeld, J. Appl. Electrochem. 22 (1992) 1–7.
[8] S. Hirano, J. Kim, S. Srinivasan, Electrochim. Acta 42 (1997) 1587.
[9] C.A. Cavalca, J.H. Arps, M. Murthy, US Patent 63,000,000B1 (2001).
[10] S. Lister, G. McLean, J. Power Sources 130 (2006) 61–76.
[11] J. St. Pierre, D.P. Wilkinson, S.A. Campbell, US Patent 6,896,792B2 (2005).
[12] S.G. Yan, J.C. Doyle, US Patent 0,163,920A1 (2005).
[13] S.G. Yan, B. Sompalli, US Patent 0,164,072A1 (2005).
[14] D. Olmeijer, US Patent 0,068,268A1 (2006).
[15] C.H. Wan, C.H. Lin, J. Power Sources 186 (2009) 229–237.
[16] J.L. Larminie, A. Dicks, Fuel Cells Systems Explained, John Wiley & Sons Ltd., 2000, p. 6, Fig. 1.6.
[17] F. Barbir, PEM Fuel Cells, Elsevier Academic Press, MA, USA, 2005 (chapter 4, p. 90, Table 4).
[18] E-Tek Co website: http://www.etek-inc.com.
[19] E.A. Ticianelli, C.R. Derouin, S. Srinivasan, J. Electroanal. Chem. 251 (1988) 275–295.
[20] S. Mukerjee, S. Srinivasan, A.J. Appleby, Electrochim. Acta 38 (12) (1993) 1661–1669.
[21] W.G.F. Grot, Nafion perfluorinated membranes product bulletin, DuPont Polymer Products Department, 1986.
[22] K.R. Cooper, V. Ramani, J.M. Fenton, H.R. Kunz, Experimental Methods and Data Analyses for Polymer Electrolyte Fuel Cells, Scribner Associates Inc., 2005.
[23] X. Yuan, H. Wang, J.C. Sun, J. Zhang, Int. J. Hydrogen Energy 32 (2007) 4365–4380.
[24] V.A. Paganin, C.L.F. Oliveira, E.A. Ticianelli, T.E. Springer, E.R. Gonzalez, Electrochim. Acta 43 (1998) 3761–3766.